A plausible molecular mechanism to explain near-infrared continuum emission: Recurrent fluorescence

O. Lacinbala, F. Calvo, E. Dartois, C. Falvo, P. Parneix, Aude Simon, T. Pino

A&A 671, A89 (2023)
https://doi.org/10.1051/0004-6361/202245421

Astronomy & Astrophysics

A plausible molecular mechanism to explain near-infrared continuum emission: Recurrent fluorescence

O. Lacinbala[1], F. Calvo[2], E. Dartois[1], C. Falvo[1,2], P. Parneix[2], A. Simon[3], and T. Pino[1]

[1] Institut des Sciences Moléculaires d'Orsay (ISMO), Université Paris-Saclay, CNRS, 598 rue André Rivière, 91405 Orsay, France
e-mail: ozan.lacinbala@universite-paris-saclay.fr; thomas.pino@universite-paris-saclay.fr
[2] Université Grenoble-Alpes, CNRS, LIPhy, 140 rue de la Physique, 38000 Grenoble, France
[3] Laboratoire de Chimie et Physique Quantiques (LCPQ), Fédération FeRMI, Université de Toulouse, CNRS, 118 route de Narbonne, 31062 Toulouse, France

Received 9 November 2022 / Accepted 22 December 2022

ABSTRACT

Context. Very small grains and large hydrocarbon molecules are known to convert a fraction of the ultraviolet (UV) and visible stellar radiation to near- and mid-infrared (IR) photons via stochastic heating and subsequent radiative de-excitation. However, no convincing explanation for the near-IR continuum emission observed in some reflection nebulae and planetary nebulae has been provided so far.
Aims. We aim to investigate the extent that recurrent fluorescence originating from stellar photon absorption by C_n ($n = 24, 42, 60$) carbon clusters can account for the IR emission detected in various interstellar environments. To this aim, we modelled the collective emission signature of a carbon cluster sample induced by irradiation from a 20 000 K blackbody source. From the obtained results, we set out to determine the fraction of interstellar carbon locked up in the emitting objects.
Methods. The collective emission signature was computationally determined for different structural families encompassing cages, flakes, pretzels, and branched isomers by means of a kinetic Monte Carlo stochastic approach based on harmonic vibrational densities of states. The collective emission spectra result from the overall radiative cooling of a large population of neutral carbon clusters, during which recurrent fluorescence and vibrational emission compete with each other.
Results. Our modelling shows that recurrent fluorescence from C_{60} cages and flakes (with little or no sp^1 carbon atoms) and C_{42} cages are able to explain the near-IR continuum emission observed in several reflection nebulae and planetary nebulae. Assuming that the continuum emission observed towards NGC 7023 is due to recurrent fluorescence induced by UV or visible photon absorption in neutral cage carbon clusters containing about 30–60 atoms, the carriers contain about 0.1–1.5% of the interstellar carbon abundance.

Key words. infrared: ISM – molecular processes – methods: numerical – ISM: abundances – ISM: molecules – ISM: lines and bands

1. Introduction

Insight into the spectroscopy and chemistry of matter in the interstellar medium (ISM) allows for better understanding of its origin and life cycle. Carbonaceous and silicate dust grains, very small grains, and polycyclic aromatic hydrocarbon-like (PAH-like) molecules are among the key potential carriers of spectral features that can enable understanding of the ISM emission in the visible as well as near-, mid-, and far-IR wavelength ranges. From astronomical observations, valuable information about the local ISM can be extracted via diagnostic tools, such as the correlation between the star formation rate and the mid-IR emission of the so-called aromatic infrared bands (AIBs) at about 3.3, 6.2, 7.7, 8.6, 11.3, and 12.7 µm (Peeters et al. 2004; Shipley et al. 2016). Physical conditions can also be inferred from specific AIB ratios (Berné et al. 2009a,b; Pilleri et al. 2012; Stock et al. 2016). A notable subset of carbonaceous interstellar matter is the large carbon clusters, for which there is growing interest due to the detection of C_{60} buckminsterfullerene in interstellar and circumstellar environments (Cami et al. 2010; Sellgren et al. 2010; Zhang & Kwok 2011; García-Hernández et al. 2012; Berné et al. 2017) and whose presence was suggested nearly 40 yr ago (Kroto et al. 1985; Foing & Ehrenfreund 1994). Possible formation processes for these large molecules in the ISM include the top-down mechanisms in which fullerenes could be formed by the shrinking of dehydrogenated PAHs (Berné & Tielens 2012; Berné et al. 2015) or produced via energetic processes affecting larger carbonaceous dust grains (Pino et al. 2019). Alternatively, a bottom-up mechanism has been suggested (closed-network growth mechanism), which could be relevant in carbon stars or supernovae environments (Dunk et al. 2012). From a spectroscopic viewpoint, cationic or neutral fullerenes, as well as fulleranes, are expected to contribute to the well-known 2175 Å UV-bump (Malloci et al. 2008; Dubosq et al. 2020) or to the diffuse interstellar bands (Cami 2014; Webster 1992; Cataldo & Iglesias-Groth 2010). Given the widespread and abundant nature of fullerenes in astrophysical environments, it is important to carefully consider all the ways in which they could contribute to observational phenomena. In this work, we focus specifically on recurrent fluorescence (RF) induced by photon absorption of fullerenes and more generally on bare carbon clusters.

The present investigation relies on a large set of neutral C_n ($n = 24, 42, 60$) carbon clusters and aims to simulate their emission spectra induced by irradiation from a 20 000 K blackbody excitation spectrum. The spectral energy distribution (SED) of a blackbody and its temperature were arbitrarily fixed to simulate the emission of a typical massive star. The molecular structures of the carbon clusters investigated in this work were obtained by systematically sampling their energy landscapes using molecular

dynamics methods based on a reactive force field (Bonnin et al. 2019) and periodic quenching using the density-functional based tight-binding (DFTB) approach (Dubosq et al. 2019). The structures obtained can be classified according to their overall shape into four main categories: cages, flakes, pretzels, and branched structures. For each of the selected sizes of 24, 42, and 60 atoms and for each of these families, up to about one thousand isomers were randomly selected from the entire sample, and their electronic excited states were computed using the time-dependent DFTB approach up to an energy of 8 eV (Dubosq et al. 2020).

Regarding the physical situation of interest in this paper, the carbon clusters are first electronically excited upon absorption of a stellar photon and very rapidly undergo several internal conversions (IC; $\sim 10^{-14}$–10^{-8} s) or intersystem crossing transitions (ISC; $\sim 10^{-10}$–10^{-7} s; Medvedev & Osherov 1995; Ermolaev 2001) before eventually reaching a ground electronic state. Electronic fluorescence is quenched by both IC and ISC processes, but because of such differences in rate constants, we focus on the IC mechanism and neglect ISC processes. The exciting photon energy is then entirely converted into vibrational motion in the ground electronic state, assuming that, for the present, the rotational energy of relatively large systems can be safely ignored. Carbon clusters, which are under scrutiny in this work, possess low-lying electronic excited states that start at ∼0.3 eV (Dubosq et al. 2020). Therefore, they are also prone to undergo inverse internal conversion (IIC; $\sim 10^{-10}$–10^{-4} s Baba et al. 1971; Chihara & Baba 1977; Nitzan & Jortner 1978, 1979; Itoh 2012) under the isolated conditions of the ISM, allowing them to become electronically excited again if the vibrational energy significantly exceeds some electronic excitation energies. Upon such circumstances, radiative relaxation occurs via vibrational emission (VE) as well as RF (also called Poincaré fluorescence Léger et al. 1988). Recently, experimental evidence has been provided for RF processes involving small molecular anions, such as C_6^- (Ebara et al. 2016; Ito et al. 2014) and C_6H^- (Ito et al. 2014), and cationic PAHs, such as the perylene (Stockett et al. 2020), naphthalene (Saito et al. 2020; Martin et al. 2017), and anthracene (Martin et al. 2013) cations.

The present investigation focuses on the near-IR continuum emission, as motived by a series of observations from several reflection and planetary nebulae in which near-IR blackbody-like emission spectra (Sellgren 1984; Phillips et al. 1984; Zhang & Kwok 1990; Otsuka et al. 2016) were reported. Duley (2009) proposed that individual carbonaceous molecules containing between ∼20 and 28 atoms, or their dimers, could account for the near-IR continuum emission and extended red emission (Lai et al. 2020; Witt & Lai 2020) via photoluminescence or thermal emission, depending on the absorbed photon energy. However, these conclusions were reached based on the experimental detection of thermal emission from either individual carbon (Mitzner & Campbell 1995; Heszler et al. 1997) or metal (Frenzel et al. 1997; Toker et al. 2007) clusters. In this work, we propose that near-IR continuum emissions could be explained by the RF mechanism originating from a large set of cage carbon clusters and, to a lesser extent, from flake structures mostly exempt from sp^1 carbon atoms. Based on this mechanism, we proceed by estimating the abundance of such carbon clusters in the observed region of NGC 7023 (Sellgren 1984).

2. Methods

Intramolecular vibrational redistribution (IVR; $\sim 10^{-13}$–10^{-7} s; Parmenter 1982; Quack 1990; Medvedev & Osherov 1995; Nesbitt & Field 1996), IC/IIC, and ISC processes can all be considered to be very fast compared to the other relaxation pathways (VE, RF, isomerisation, and dissociation), and we assume that between two successive photon emissions, the vibrational energy is statistically distributed among all accessible vibronic states at each instant of the radiative relaxation. This assumption allows us to use microcanonical statistical mechanics to determine RF and VE rate constants under isolated and equilibrium conditions. In the harmonic approximation, the vibrational densities of states needed for these quantities can be exactly obtained from the knowledge of the vibrational frequencies by direct counting (Beyer & Swinehart 1973). A kinetic Monte Carlo (kMC) method was implemented to sample the possible relaxation pathways from which the emission spectrum was obtained by summing over all radiative processes. Models for the competition between RF and VE mechanisms in carbon clusters have already been presented and discussed in a previous study (Lacinbala et al. 2022). In particular, the specific contributions of VE and RF mechanisms were highlighted by repeating the kMC trajectories without considering dissociation and isomerisation processes. A similar approach was used in this work. In the following paragraphs, we detail the specific features that are new in the model with respect to our previous work (Lacinbala et al. 2022), which assumed the carbon clusters to be isolated.

In this work, we assumed the large carbon clusters to be irradiated by a 20 000 K blackbody SED, which simulates the illumination received from a B star (Appendix A). Determining the cooling cascades following all possible photon excitations from the whole SED would be too computationally expensive. Then, the method we used is explained as follows. During the kMC trajectory, the internal energy decreases, and the integration proceeds until no more excess energy is left in the system, and thus it becomes frozen in its vibrational and electronic ground states. By accumulating emitted photons over multiple trajectories, we obtained information over the entire excess energy range between zero and the initial photon energy chosen to excite the system. It was thus possible to impose a fixed but large value for the excitation energy and produce more realistic emission spectra after convolution of the energy-resolved spectra with the SED.

We denote by $N(\nu, E)$ the total number of photons with energy $h\nu$ emitted from an ensemble of molecules with a given chemical composition and a fixed structure initially excited at energy E. The quantity $N(\nu, E)$ includes all the emitted photons accumulated along the radiative cascade, from the initial excitation energy E up to the point where the molecules have no residual energy left. Our aim was to evaluate the total number $F(\nu)$ of photons emitted by a set of such molecules initially excited by a distribution of energy $P(E)$ and resolved by the photon energy $h\nu$:

$$F(\nu) = \int_0^\infty \mathrm{d}E\, N(\nu; E) P(E). \tag{1}$$

To this end, we began by introducing the microcanonical emission spectrum $n(\nu, E)$ corresponding to the derivative of $N(\nu, E)$ with respect to energy,

$$n(\nu, E) = \frac{\mathrm{d}N(\nu; E)}{\mathrm{d}E}, \tag{2}$$

such that $\mathrm{d}N(\nu, E) = n(\nu, E)\mathrm{d}E$ is the number of photons of energy $h\nu$ directly emitted from molecules within the energy shell between E and $E + dE$. The total number of emitted photons from a set of molecules excited by the excess energy distribution

$P(E)$ could thus be rewritten as

$$F(\nu) = \int_0^\infty \mathrm{d}E \int_0^E \mathrm{d}E'\; n(\nu, E')P(E), \tag{3}$$

or, changing the limits of integration, as

$$\begin{aligned} F(\nu) &= \int_0^\infty \mathrm{d}E' \int_{E'}^\infty \mathrm{d}E\; n(\nu, E')P(E) \\ &= \int_0^\infty \mathrm{d}E'\; n(\nu, E')K(E'), \end{aligned} \tag{4}$$

where we have introduced $K(E')$ as the total probability that a molecule was initially excited with an energy larger than E'. This function is explicitly given by

$$K(E') = \int_{E'}^\infty \mathrm{d}E\; P(E). \tag{5}$$

The probability density of having a system excited at energy E' can be expressed with the SED $u(E';T)$ and the electronic absorption cross-section $C_{\mathrm{abs}}(E')$ through

$$P(E) = \frac{u(E;T)/EC_{\mathrm{abs}}(E)}{\int_0^\infty \mathrm{d}E'\; u(E';T)/E'C_{\mathrm{abs}}(E')}, \tag{6}$$

where $u(E';T)/E'$ is the spectral photon number density per unit volume. The product of these two quantities determines the relative propensity of selectively exciting the molecule at energy E'. In the present work, electronic absorption cross-sections were determined from electronic oscillator strengths of carbon clusters. Below 8.2 eV electronic energy, these quantities were obtained by Dubosq et al. (2020) using simple quantum calculations, whereas for high electronic energy (>8 eV), the model of Li & Draine (2001) was used (see Appendix A for more details; in particular Fig. A.3 shows the typical internal energy dependence of the quantity $K(E)$ obtained using an SED corresponding to 20 000 K blackbody emission). In practice, the microcanonical emission spectrum is discretised both in photon energy $h\nu$ and in internal energy E using regular bin sizes of 1 cm^{-1} in both variables.

The molecules were initially excited at an upper value of energy corresponding to the ionisation threshold of carbon clusters, and we set the C_{60} ionisation threshold to be that of the buckminsterfullerene, which is known to be around 7.5 eV (De Vries et al. 1992), irrespective of their structures. For smaller clusters, we took a slightly higher ionisation threshold, 8.0 eV for C_{42} clusters and 8.5 eV for C_{24} clusters, as suggested in Seifert et al. (1996); Bach & Eyler (1990).

The abundance of cationic carbon clusters are expected to be comparable to that of neutral carbon clusters. For instance, Iglesias-Groth (2019) deduced an ionisation fraction of 20% for buckminsterfullerene in the IC 348 star-forming region, and Murga et al. (2022) found that this fraction is mostly less than 80% in the Orion Bar. However, owing to their rather large size and the spreading of the extra charge over the entire carbon mesh, we did not expect significant changes in the vibrational or electronic structures, at least from the statistical perspective that we adopted in this work. Moreover, we expected the relative propensities for cations over neutrals to depend quite significantly on the physical and chemical environment. In addition to being out of reach, a correct modelling of the ionisation yield (Jochims et al. 1996; Verstraete et al. 1990) was not expected to improve our model by a large extent. For simplifying purposes, and without altering our general conclusions regarding the photochemistry, we thus assumed that the ionisation yields equal unity above the ionisation threshold.

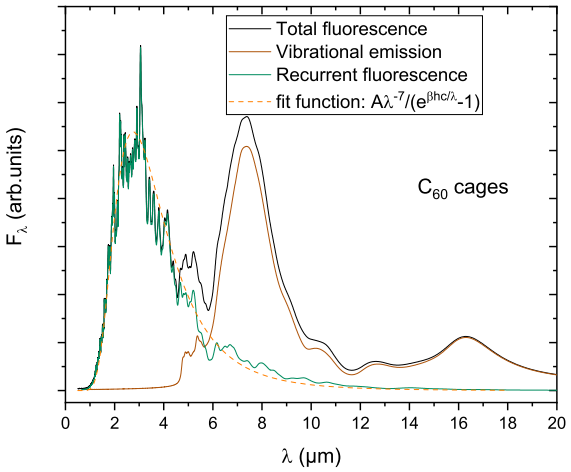

Fig. 1. Collective emission intensity spectrum from 1000 C_{60} cage carbon cluster sample irradiated by a 20 000 K blackbody excitation and convoluted with a Lorentzian function with a FWHM of 200 cm^{-1}.

For each system, a series of 2×10^5 independent kMC trajectories were performed to compute $n(\nu, E)$. Finally, the total emission spectrum was obtained for a specific SED using Eq. (4). The fixed discretisation chosen for the microcanonical emission spectrum led to some numerical errors at low energy and a minor dependence on the initial excess energy, which we evaluated as not to exceed 5% on the total number of emitted photons.

Carbon cluster structures formed in ISM conditions are assumed to be out of equilibrium, which allowed us to take a uniform distribution of isomers. In addition to radiative processes, electronically excited carbon clusters can also dissociate, isomerise, and even ionise. Isomerisation processes were implicitly accounted for by assuming a broad, uniform sample of structures over which our results were averaged. Ionisation from neutral clusters is another possible decay relaxation pathway, although it requires substantial excess energy. As mentioned, ionisation imposes an upper limit onto the maximum excitation energy that can be considered for the radiative processes. Finally, the most likely dissociation pathway for the carbon clusters is C_2 dissociation, but again such processes were shown to be negligible for C_{60} at excitation energies lower than 7.5 eV (Lifshitz 2000).

3. Results

3.1. Emission spectra from carbon cluster samples

The total emission spectrum from the sub-sample of cage structures of C_{60} upon irradiation by a 20 000 K blackbody stellar-like spectrum is shown in Fig. 1. From our modelling, we find that the broad emission bands above 5 μm wavelength are essentially due to VE processes, whereas the broad emission band below 5 μm wavelength is exclusively due to RF processes. The RF part of the emission spectrum is a blackbody-like emission, which can be explained as follows: For any carbon cluster, vibrational energy allows electrons to be promoted to upper electronic states. Thus, vibrational energy can be considered as a finite heat bath for accessible electronic states. The occupation of the continuum of electronic states over the whole carbon cluster sample can be thought of as a 'thermal' excitation and thus accounts for the

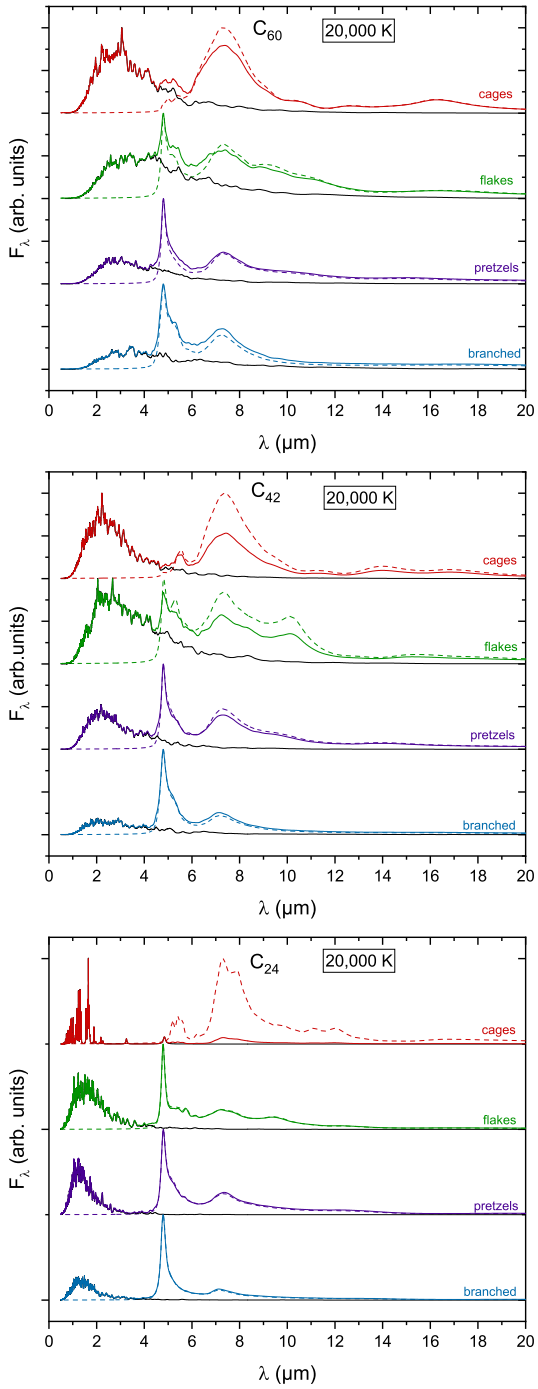

Fig. 2. Normalised emission intensity spectra as a function of the wavelength from the four families of cages, flakes, pretzels, and branched structures and the three carbon cluster sizes of 60, 42, and 24 carbon atoms upon irradiation by a 20 000 K star-like SED. The dashed lines highlight the corresponding spectra in which RF processes are ignored. The specific contribution of RF processes is highlighted as black lines.

blackbody-like emission spectrum of RF. A given carbon cluster emits a discrete spectrum, but the collective emission of carbon clusters gives rise to continuum emission spectra in which the RF part has a blackbody-like shape. The blackbody-like fit of the recurrent fluorescence contribution in Fig. 1 indicates a temperature of 747 K.

Figure 2 shows the entire set of emission spectra obtained for the four structural families of C_{60}, C_{42}, and C_{24} carbon clusters irradiated by a 20 000 K star-like SED. As can be seen in this figure, the VE part of the emission spectrum depends on the underlying structural family, in contrast to the RF part, which always shows the same overall blackbody-like shape (Fig. 2). In the figure, the maximum of the RF part (<5 μm) for all families appears clearly blueshifted as carbon clusters become smaller. This maximum was found between 2 and 4 μm for C_{60} and falls below 2 μm for C_{24}. The emission intensity spectrum from C_{24} cages is particularly different and notably more structured because there are only 11 such conformers.

Noticeably, RF leads to stronger relative intensity emission of low-frequency modes (emission bands above 4 μm) because RF occurs mainly at internal energies higher than 2.5 eV (Lacinbala et al. 2022) but also because, and especially at high internal energies, VE occurs mainly through high-frequency modes. At high energies, RF therefore competes with emission from high-frequency vibrational modes. We thus generally expected that RF should predominantly reduce the relative intensity of high-frequency modes and enhance the relative intensities of low-frequency modes. However, RF can still considerably emit beyond 5 μm (Fig. 1), which prevented us from attempting oversimplified analyses.

The relative VE intensity bands also depend on the exciting SED because absorbed photon energies are converted into internal energy of carbon clusters, which affects the RF efficiency (Lacinbala et al. 2022). This is illustrated when comparing results on emission spectra induced by irradiation from the standard interstellar radiation field (ISRF) with that induced by a star with a $T_{\rm eff}$ = 20 000 K (Fig. B.1).

3.2. Carrier size estimations in NGC 7023

The NGC 7023 is a bright reflection nebula located in the Cepheus constellation at about 400 pc. The illumination of the cloud by the HD 200775 Herbig B2Ve star enables exploration of the physical properties of its dust grains. In such an environment, as stated by Sellgren (1984), the observed near-IR emission cannot be explained by reflected light, fluorescence, faint stars, free-free emission, or by thermal emission from dust in equilibrium with the stellar radiation field. In this section, we calculate the carrier sizes constrained by astronomical observations under the hypothesis that the near-IR emission arises from the RF of the carbon cluster carriers.

Figure 2 shows the emission spectra of carbon cluster samples in the near-IR region in semi-log scale for the four families of C_{60} and for C_{42} cages. We have already shown that below 4 μm, emission is due to RF processes. Comparing the spectra obtained for the different structural families suggests that the broad band emission seen at 4.8 μm in Fig. 3a stems from vibrational mode emission involving sp^1 carbon atoms, which are essentially absent in cages. Such a band at 4.8 μm is not astrophysically observed, providing a strong indication that pretzel and branched structures explored in this study, and even flake structures that contain some sp^1 dangling atoms, can be safely discarded from the interpretation (Flagey et al. 2006; Onaka et al. 2018).

Figure 3 highlights the emission spectra from all structural families of C_{60} and from the cages of C_{42}, in comparison to C_{60}, in the near-IR range (1–5 μm). The spectra were normalised so their integral equals unity. The radiated energy via RF was estimated to be about 18% of the total radiated energy for C_{60} cages, about 25% for flakes, 14% for pretzels, and 13% for branched structures. For C_{42} cages, this percentage is about 21.5%. The emission spectra in Fig. 3b are very similar to the near-IR continuum emission spectrum observed towards NGC 7023 (at a

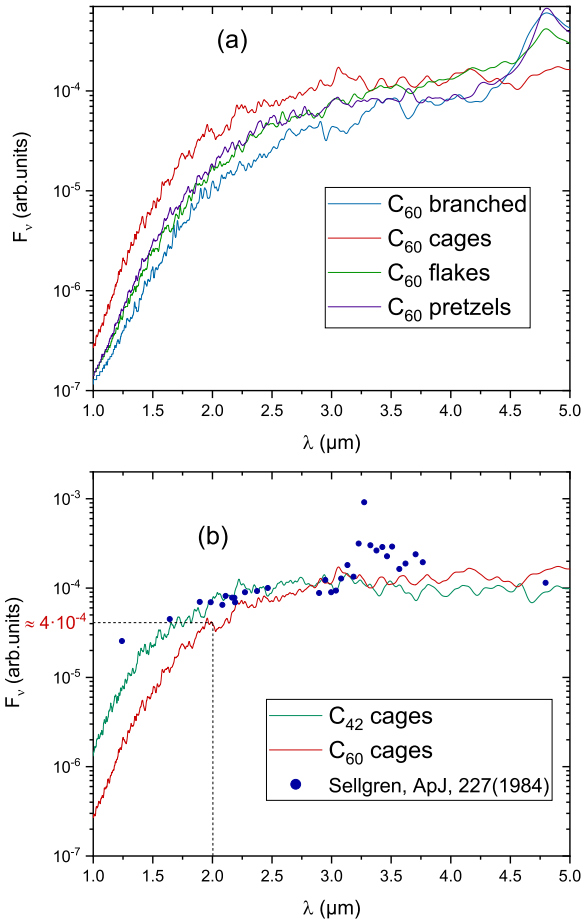

Fig. 3. Emission spectra of carbon cluster samples in the near-IR region. Note that F_ν is displayed as a function of wavelength, as in Sellgren (1984). The spectra are normalised so the integrated emission is unity. Upper panel: spectra obtained for the four families of C_{60}. Lower panel: spectra obtained for the cage families of C_{60} and C_{42}. The dashed lines emphasise the relative value of emission intensity of C_{60} cage sample at 2 μm. Observational data of the NGC 7023 reflection nebulae at 30″W 20″N position, as extracted from Sellgren (1984), are shown as blue dots.

position 30″ west 20″ north of HD 200775) by Sellgren (1984), showing a continuum emission signal from 5 to 2.5 μm (in semi-log scale) and a steep decrease below 2 μm, reflecting the exponential decay of the blackbody-like emission due to RF.

From Fig. 5 of Sellgren (1984) and the simulated emission spectra of Fig. 3b, we deduced intensity ratios between the plateau and the descent of the continuum at several frequencies (given in Table 1). The larger ratios were found for the cage isomers, with the steepest descent below 2 μm. The evolution of the intensity ratios, with the cluster size reported in Table 1, show that the continuum emission around 1.25 μm is mainly due to clusters containing less than 40 carbon atoms. Around 2.25 μm, clusters containing up to about 60 carbon atoms could carry the emission. However, our sample of C_{24} cage clusters is far too small (there are only 11 in our sample) and cannot be conclusively considered to contribute to the continuum emission.

If carbon clusters were the carriers of the near-IR continuum emission, then cages containing about 30–60 atoms would be the best candidates. Below 30 atoms, the cage clusters would be in minority relative to other families (especially flakes), while above 60 atoms, the cages would be too cold to emit substantially in the near-IR region.

Table 1. Intensity ratios between the continuum emission at 4.8 μm and emission at 1.25, 1.75, and 2.25 μm from NGC 7023 observation (Sellgren 1984) and from the simulation (Fig. 3b).

	NGC 7023	C_{60} cages	C_{42} cages
$I_{1.25\,\mu m}/I_{plateau}$ ($\times 10^{-2}$)	20	1.3	8.3
$I_{1.75\,\mu m}/I_{plateau}$ ($\times 10^{-2}$)	33	6.3	50
$I_{2.25\,\mu m}/I_{plateau}$ ($\times 10^{-2}$)	50	50	10

Notes. Ratios for NGC 2023 are similar to those of NGC 7023 (Sellgren 1984).

3.3. Estimation of abundances

In this section, we turn to estimating the abundance of cage carbon clusters required to explain the near-IR continuum emission in NGC 7023. Observations from Sellgren (1984) indicate that the near-IR spectral emittance around the wavelength of 2 μm (chosen arbitrarily) is about 20 mJy within a 12″ diaphragm aperture.

Assuming that over the C_{60} cage carbon cluster sample the total absorbed power density (W m^{-2}) is equal to the total emitted power density, the computed emission spectrum integrated over frequencies would be equal to the absorbed power density integrated over exciting energies. This assumption is supported by the low densities, making relaxation necessarily go through photon emission. The emitted emission spectrum of C_{60} cages in the near-IR wavelength range is shown in Fig. 3b in such a way that the integral over the frequency is set to unity. From the electronic absorption cross-section of the C_{60} cage carbon cluster sample (see Appendix A), we can also estimate the absorbed power flux density.

Keeping in mind that the integral of the emission spectrum shown in Fig. 3 is normalised, we show in Appendix C that the spectral power density that should be detected on Earth is obtained by multiplying the y-axis of Fig. 3b by the following quantity:

$$\frac{1}{4\pi}\left(\frac{R_\triangle}{D_\triangle}\right)^2\left(\frac{R_\star}{D_\star}\right)^2 n_C^{2/3}\int_0^{E_{ion}} \mathrm{d}E\; u^\circ(E;T)C_{abs}(E), \tag{7}$$

with u° (W m^{-2} Hz^{-1}) as the spectral emittance of the blackbody (star) at temperature T_{eff} = 20 000 K, $R_\star$ as the radius of the illuminating source, $D_\star$ as the distance between the illuminating source and NGC 7023, C_{abs} (m^2) as the electronic absorption cross-section of the set of C_{60} cage carbon clusters, n_C (m^{-3}) as the C_{60} cages volume density in the observed region, $R_\triangle$ as the spatial extension of the observed NGC 7023 region, $D_\triangle$ as the distance between Earth and NGC 7023, and E_{ion} as the mean ionisation threshold of C_{60} cages set to 7.5 eV for C_{60} cages and 8 eV for C_{42} cages, acting as an upper limit of integration. For C_{60} cages, the quantity expressed in Eq. (7) led to $2.3\times10^{-27}\times n_C^{2/3}$ W m^{-2} sr^{-1} (see Appendix C for details on this derivation). In Fig. 3b, the relative emission at 2 μm frequency represents a fraction of 4×10^{-5} of the total emission. Thus, the detected spectral power density on Earth is equal to

$$4\times10^{-5}\times2.3\times10^{-27}\times n_C^{2/3}\approx 0.01\times n_C^{2/3}\,\mathrm{mJy\,sr^{-1}}. \tag{8}$$

Assuming that the observed region is spherical, the detected ratio of the emitted power over all directions is $2\pi\cos\alpha/4\pi$, with α being the telescope aperture equal to 12″. Thus, the detected power from Earth is $6.3\times10^{-2}n_C^{2/3}$ mJy. Given that

Sellgren (1984) detected 20 mJy at 2 μm, it follows that $n_C \approx 6 \times 10^{-3}$ cm^{-3}.

The hydrogen abundance in this region is ~10^5 cm^{-3} (Martini et al. 1999), carbon being in abundance of ~2.4×10^{-4} relative to hydrogen (Cardelli et al. 1996). It follows that the above calculations require 1.5% of the carbon to be locked up as neutral C_{60} cages to explain the level of intensity observed in the NGC 7023 line of sight. Repeating the calculation for C_{42} cages yields 0.35%. From this analysis, 0.1–1.5% of the elemental carbon of the region should be locked up in these neutral cage carbon clusters.

Finally, considering cationic systems, they should be able to sustain higher excitation energies because their ionisation threshold is higher than those of neutrals clusters (Buntine et al. 2021; Rademacher et al. 2022). The extra positive charge that is diluted over the entire structure makes the IR spectrum of the cationic carbon cluster sample mostly unchanged compared to neutral species (Dubosq et al. 2019), as already reported for PAH compounds (Bauschlicher et al. 2009). By the same token, we expect optical spectra to be similar for cationic and neutral carbon cluster samples. Therefore, the blackbody-like RF spectrum would correspond to a higher temperature, indicating that cationic carriers would be slightly larger than the neutrals clusters.

4. Discussion

Otsuka et al. (2016) observed near-IR excess continuum emission in the planetary nebulae Lin49 and deduced, via blackbody fit and classical thermodynamic calculations, that the carriers should contain less than 39 carbon atoms. These authors stressed that at such sizes, there are not enough vibrational modes to reproduce the broad blackbody continuum emission. However, the present work shows that stochastic heating of a large set of structurally diverse isomers leads to a blackbody-like emission via RF.

Given that the maximum emission of the blackbody-like emission in Fig. 12 in Otsuka et al. (2016) peaks around 2.1 μm, we deduced from Fig. 2 of our work that neutral cages, possibly together with flakes without dangling sp^1 atoms and containing approximately 42 carbon atoms, could be the carriers of the near-IR excess continuum emission reported by Otsuka et al. (2016). In addition, the continuum emission responsible for the differential spectrum in Fig. 12 of Otsuka et al. (2016) could be assigned to neutral cages or flake clusters containing ~60 carbon atoms.

The percentage of interstellar carbon locked up specifically in C_{60} buckminsterfullerene has been estimated to be 0.1–0.6% in NGC 7023 (Sellgren et al. 2010) in a region 25″ north-east of the exciting star (HD200775), based on the C_{60} VE bands observed at 7.0, 8.5, 17.4, and 18.9 μm in NGC 7023. When related to our findings, this means that the percentage of buckminsterfullerenes among C_{60} cages should be 6–30%. However, our calculation corresponds to a region located at 35″ north-west of the exciting star. Berné & Tielens (2012) estimated that 0.001% of the carbon is locked up as buckminsterfullerenes located 35″ north-east of the exciting star, implying that 0.2% of cage carbon clusters are buckminsterfullerenes. We stress that C_{60} buckminsterfullerene does not contribute to the near-IR emission because for this very specific cluster, RF is negligible due to rather high first electronic excited state energy (around 2.0 eV (Haufler et al. 1991) above the ground state). However, astronomical observations show buckminsterfullerene emission bands and near-IR continuum emission to all be present in the same region. The correlation of these emissions could provide valuable information about the nature of the formation mechanisms of buckminsterfullerene.

This work reveals that any family species with low-lying excited electronic states in ISM conditions should emit a blackbody-like spectrum. Besides pure carbon clusters, large PAHs could also be the carriers of near-IR continuum emission because their electronic absorption cross-sections are of the same order of magnitude as that of carbon clusters (Li & Draine 2001). In particular, the near-IR continuum emission from PAHs should be correlated to the 3.3 μm emission band and to the AIBs. It thus seems important for radiative models describing the evolution and emission of PAHs and Very Small Grains to also account for the RF mechanism.

Recurrent fluorescence has also been suspected to contribute to the extended red emission (ERE) through large species with low-lying electronic states. The ERE is a broad emission band peaking between 600 and 850 nm with a full width at half maximum (FWHM) spanning between 60 and 120 nm (Witt & Lai 2020; Lai et al. 2020). The RF part of the emission spectra is always blackbody-like, unlike ERE. We conclude that RF from broad samples of isomers cannot be the only mechanism for explaining ERE. However, RF cannot be entirely ruled out as one of the competing radiative pathways for ERE, as Duley (2009) proposed that carbonaceous molecules containing 20–28 carbon atoms can be the carriers of ERE and near-IR continuum via either photoluminescence or thermal emission of their dimers. Furthermore, a recent investigation related to the stabilizing effect of RF against photo-thermo-dissociation (Iida et al. 2022) allows us to speculate that RF from smaller individual carbon clusters containing fewer than 24 atoms can occur with collective emission that would give rise to blackbody-like emission in the visible range and thereby contribute to ERE.

5. Conclusions

The present work reveals that the collective emission spectra induced by a stellar blackbody SED with effective temperature $T_{\rm eff} \approx 20\,000$ K originating from a large set of carbon clusters spreads from the far- to the near-IR wavelength region. By inhibiting the emission from high-frequency vibrational modes, RF turns out to also have a significant impact on the vibrational contribution to the emission spectra. Of the carbon clusters scrutinised, between 10% and 25% of the total absorbed energy was radiated via RF, depending on the size and structural family. Furthermore, the RF component of collective emission spectra has a blackbody-like shape for all structural families and sizes in the range of 24–60 atoms studied in this work.

The observed near-IR emission in some reflection and planetary nebulae can be explained by RF from a large set of C_{60} or C_{42} cages and flakes (free from sp^1 carbon atoms). Under such circumstances, the near-IR continuum observed in NGC 7023 (Sellgren 1984) was estimated as being due to carbon clusters containing mainly between 30 and 60 carbon atoms, with 0.1–1.5% of the elemental carbon being locked up in these carriers.

The RF from large PAHs with low-lying electronic states could also contribute to the near-IR continuum emission, and its correlation to AIBs would be worth investigating further. Considering that PAHs are stabilised over cages due to a few extra hydrogen atoms (Perez-Mellor et al. 2022; Lepeshkin et al. 2022), applying the present statistical framework to those compounds would appear to be a natural extension of this work.

Acknowledgements. Financial support by the Agence Nationale de la Recherche (ANR) project "PACHYNO" ANR-16-CE29-0025 is gratefully acknowledged. O.L. acknowledges Prof. Cami for his valuable comments on this work and the Centre National de la Recherche Scientifique (CNRS) for funding.

References

Baba, H., Nakajima, A., Aoi, M., & Chihara, K. 1971, J. Chem. Phys., 55, 2433
Bach, S. B., & Eyler, J. R. 1990, J. Chem. Phys., 92, 358
Bauschlicher, C. W., Peeters, E., & Allamandola, L. J. 2009, ApJ, 697, 311
Berné, O., & Tielens, A. G. 2012, PNAS, 109, 401
Berné, O., Fuente, A., Goicoechea, J., et al. 2009a, ApJ, 706, L160
Berné, O., Joblin, C., Fuente, A., & Ménard, F. 2009b, A&A, 495, 827
Berné, O., Montillaud, J., & Joblin, C. 2015, A&A, 577, A133
Berné, O., Cox, N., Mulas, G., & Joblin, C. 2017, A&A, 605, A1
Beyer, T., & Swinehart, D. 1973, Commun. ACM, 16, 379
Bonnin, M. A., Falvo, C., Calvo, F., Pino, T., & Parneix, P. 2019, Phys. Rev. A, 99, 042504
Buntine, J. T., Cotter, M. I., Jacovella, U., et al. 2021, J. Chem. Phys., 155, 214302
Cami, J. 2014, Proc. Int. Astron. Union, 9, 370
Cami, J., Bernard-Salas, J., Peeters, E., & Malek, S. E. 2010, Science, 329, 1180
Cardelli, J. A., Meyer, D. M., Jura, M., & Savage, B. D. 1996, ApJ, 467, 334
Cataldo, F., & Iglesias-Groth, S. 2010, Fulleranes: The Hydrogenated Fullerenes, 2 (Springer Science & Business Media)
Chihara, K., & Baba, H. 1977, Chem. Phys., 25, 299
De Vries, J., Steger, H., Kamke, B., et al. 1992, Chem. Phys. Lett., 188, 159
Dubosq, C., Falvo, C., Calvo, F., et al. 2019, A&A, 625, A11
Dubosq, C., Calvo, F., Rapacioli, M., et al. 2020, A&A, 634, A62
Duley, W. 2009, ApJ, 705, 446
Dunk, P. W., Kaiser, N. K., Hendrickson, C. L., et al. 2012, Nat. Commun., 3, 1
Ebara, Y., Furukawa, T., Matsumoto, J., et al. 2016, Phys. Rev. Lett., 117, 133004
Ermolaev, V. L. 2001, Russ. Chem. Rev., 70, 471
Flagey, N., Boulanger, F., Verstraete, L., et al. 2006, A&A, 453, 969
Foing, B., & Ehrenfreund, P. 1994, Nature, 369, 296
Frenzel, U., Hammer, U., Westje, H., & Kreisle, D. 1997, Zeitsch. Physik D Atoms Mol. Clusters, 40, 108
García-Hernández, D. A., Villaver, E., García-Lario, P., et al. 2012, ApJ, 760, 107
Haufler, R., Chai, Y., Chibante, L., et al. 1991, J. Chem. Phys., 95, 2197
Heszler, P., Carlsson, J., & Demirev, P. 1997, J. Chem. Phys., 107, 10440
Iglesias-Groth, S. 2019, MNRAS, 489, 1509
Iida, S., Hu, W., Zhang, R., et al. 2022, MNRAS, 514, 844
Itoh, T. 2012, Chem. Rev., 112, 4541
Ito, G., Furukawa, T., Tanuma, H., et al. 2014, Phys. Rev. Lett., 112, 183001
Jochims, H., Baumgärtel, H., & Leach, S. 1996, A&A, 314, 1003
Kroto, H. W., Heath, J. R., O'Brien, S. C., Curl, R. F., & Smalley, R. E. 1985, Nature, 318, 162
Lacinbala, O., Calvo, F., Dubosq, C., et al. 2022, J. Chem. Phys., 156, 144305
Lai, T. S., Witt, A. N., Alvarez, C., & Cami, J. 2020, MNRAS, 492, 5853
Léger, A., Boissel, P., & d'Hendecourt, L. 1988, Phys. Rev. Lett., 60, 921
Lepeshkin, S. V., Baturin, V. S., Naumova, A. S., & Oganov, A. R. 2022, J. Phys. Chem. Lett., 13, 7600
Li, A., & Draine, B. 2001, ApJ, 554, 778
Lifshitz, C. 2000, Int. J. Mass Spectrom., 198, 1
Malloci, G., Mulas, G., Cecchi-Pestellini, C., & Joblin, C. 2008, A&A, 489, 1183
Martin, S., Bernard, J., Brédy, R., et al. 2013, Phys. Rev. Lett., 110, 063003
Martin, S., Matsumoto, J., Kono, N., et al. 2017, Nucl. Instrum. Methods Phys. Res. B: Beam Interact. Mater. At., 408, 209
Martini, P., Sellgren, K., & DePoy, D. 1999, ApJ, 526, 772
Mathis, J., Mezger, P., & Panagia, N. 1983, A&A, 128, 212
Medvedev, E. S., & Osherov, V. I. 1995, Springer Series in Chemical Physics (Berlin: Springer-Verlag)
Mitzner, R., & Campbell, E. E. 1995, J. Chem. Phys., 103, 2445
Murga, M., Akimkin, V., & Wiebe, D. 2022, MNRAS, 517, 3732
Nesbitt, D. J., & Field, R. W. 1996, J. Phys. Chem., 100, 12735
Nitzan, A., & Jortner, J. 1978, Chem. Phys. Lett., 60, 1
Nitzan, A., & Jortner, J. 1979, J. Chem. Phys., 71, 3524
Onaka, T., Nakamura, T., Sakon, I., et al. 2018, ApJ, 853, 31
Otsuka, M., Kemper, F., Leal-Ferreira, M. L., et al. 2016, Proc. Int. Astron. Union, 12, 254
Parmenter, C. S. 1982, J. Phys. Chem., 86, 1735
Peeters, E., Spoon, H., & Tielens, A. 2004, ApJ, 613, 986
Perez-Mellor, A. F., Parneix, P., Calvo, F., & Falvo, C. 2022, J. Chem. Phys., 157, 171102
Phillips, J., Sanchez Magro, C., & Martinez Roger, C. 1984, A&A, 133, 395
Pilleri, P., Montillaud, J., Berné, O., & Joblin, C. 2012, A&A, 542, A69
Pino, T., Chabot, M., Béroff, K., et al. 2019, A&A, 623, A134
Pogodin, M. A., Miroshnichenko, A. S., Tarasov, A. E., et al. 2004, A&A, 417, 715
Quack, M. 1990, Annu. Rev. Phys. Chem., 41, 839
Rademacher, J., Reedy, E. S., & Campbell, E. K. 2022, J. Phys. Chem. A, 126, 2127
Saito, M., Kubota, H., Yamasa, K., et al. 2020, Phys. Rev. A, 102, 012820
Seifert, G., Vietze, K., & Schmidt, R. 1996, J. Phys. B: At. Mol. Opt. Phys., 29, 5183
Sellgren, K. 1984, ApJ, 277, 623
Sellgren, K., Werner, M. W., Ingalls, J. G., et al. 2010, ApJ, 722, L54
Shipley, H. V., Papovich, C., Rieke, G. H., Brown, M. J., & Moustakas, J. 2016, ApJ, 818, 60
Stock, D., Choi, W.-Y., Moya, L., et al. 2016, ApJ, 819, 65
Stockett, M. H., Bull, J. N., Buntine, J. T., et al. 2020, J. Chem. Phys., 153, 154303
Toker, Y., Aviv, O., Eritt, M., et al. 2007, Phys. Rev. A, 76, 053201
Van den Ancker, M., Djie, T. A., Catala, C., et al. 1997, A&A, 324, L33
Verstraete, L., Léger, A., d'Hendecourt, L., Defourneau, D., & Dutuit, O. 1990, A&A, 237, 436
Webster, A. 1992, MNRAS, 255, 41P
Witt, A. N., & Lai, T. S.-Y. 2020, Astrophys. Space Sci., 365, 1
Zhang, C., & Kwok, S. 1990, A&A, 237, 479
Zhang, Y., & Kwok, S. 2011, ApJ, 730, 126

Appendix A: Absorption cross-section and SED

The two spectral irradiances used in this work are depicted in Figure A.1 as a function of photon energy. The ionisation threshold at 7.5 eV is highlighted in the figure (excitations above this threshold were not considered in our modelling for neutral carbon clusters).

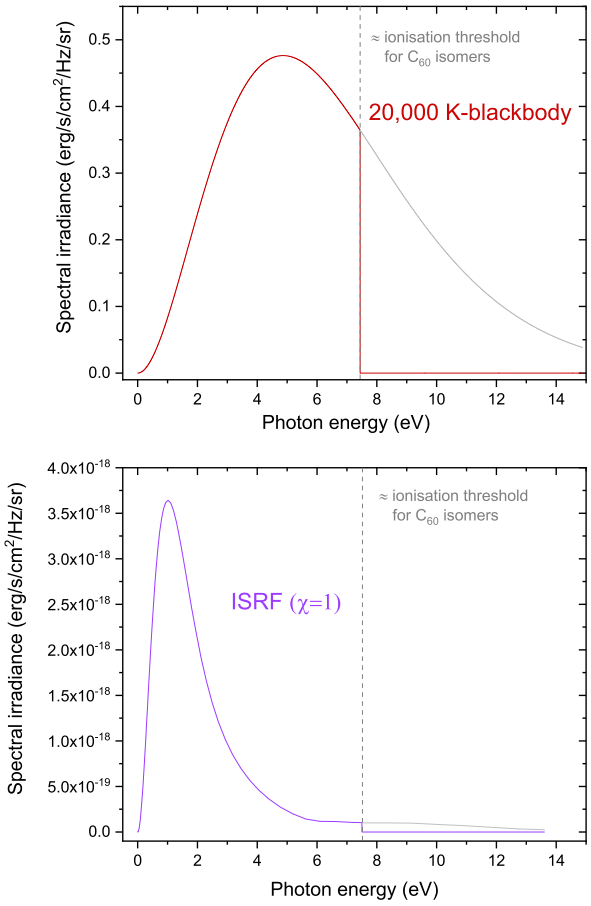

Fig. A.1: Spectral irradiance associated with SEDs used in this work. The functions are cut at the ionisation threshold, shown here at 7.5 eV for C_{60}. Left panel: Spectral irradiance at the surface of a 20,000 K blackbody. Right panel: Spectral irradiance of the $\chi = 1$ ISRF from Mathis et al. (1983).

In Dubosq et al. (2020), the electronic oscillator strength of all $S_n \rightarrow S_0$ transitions were determined using the time-dependent DFTB approach. The absorption cross-sections were obtained, as displayed in Figure A.2 for C_{60} cage isomers.

The electronic oscillator strengths extracted from Dubosq et al. (2020) are not as reliable above 8.2 eV, and the absorption cross-sections were instead fitted by Draine and Li's model Li & Draine (2001) above 8.2 eV. This adjustment led to a small computational artefact, manifested as a discontinuity in Fig. A.2, but it does not influence the results and conclusions of this work to any appreciable extent. Figure A.3 shows the typical variations of the probability $K(E)$ with increasing excess energy, as deduced from Eq. 5, for several randomly chosen clusters from the C_{60}, C_{42}, and C_{24} samples.

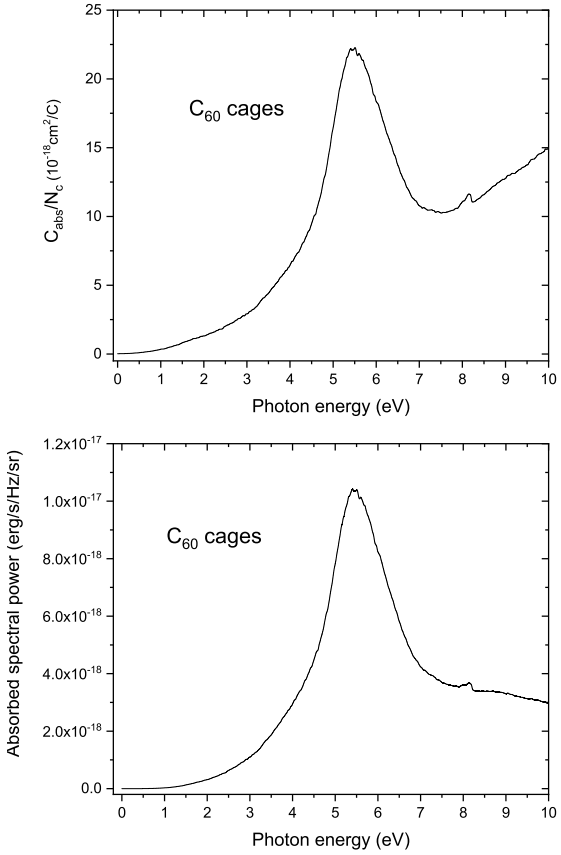

Fig. A.2: Left panel: The average electronic absorption cross-section per carbon number of C_{60} cage isomers obtained by a FWHM= 300 cm^{-1} Lorentzian convolution. Right panel: The average absorbed spectral energy power by C_{60} cages located at the surface a 20,000 K blackbody. These curves were obtained by multiplying the 20,000 K blackbody spectral irradiance shown in Figure A.1 and the average electronic absorption cross-section of C_{60} cage isomers shown at the left panel.

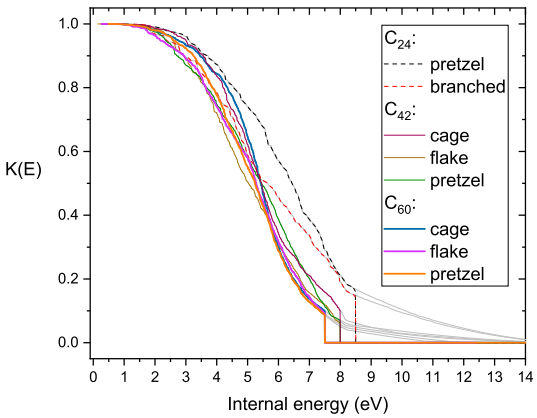

Fig. A.3: Probability $K(E)$ that individual, randomly chosen carbon clusters were excited with an energy of at least E for an excitation from a 20,000 K blackbody star, as a function of E. The cutoff values at 7.5, 8.0, and 8.5 eV appropriate for C_{60}, C_{42}, and C_{24} isomers, respectively, were imposed as an approximate way of accounting for ionisation processes.

Appendix B: Emission spectra induced by χ=1 ISRF irradiation

The emission spectra from large sets of carbon clusters irradiated by the 20,000 K blackbody (star-like SED) and the standard interstellar radiation field ($\chi = 1$) are shown in Figure B.1. Overall, the spectra are very similar, including the relative contribution from RF. However, the most noticeable differences are found for the spectra from pretzel and branched conformers of the larger clusters C_{42} and C_{60} at low frequencies.

That the differences are stronger at low frequencies is a mere consequence of the 20,000 K blackbody SED being more extended towards higher energies relative to the ISRF irradiation density (see Fig. A.1). The higher internal energy experienced by the clusters produces a greater amount of VE from high-frequency modes Lacinbala et al. (2022) and a concomitantly lower contribution from low-frequency modes, which is precisely what is found in Fig. B.1.

Appendix C: Calculation of the detected emission power density from C_{60} cages in NGC 7023

In this section, we discuss in more detail the derivation of Eq. 7 and its numerical implementation. The exciting power density per frequency in the observed region is given by the following quantity

$$\left(\frac{R_\star}{D_\star}\right)^2 \times u^\circ(\nu; T), \tag{C.1}$$

with u° ($\mathrm{W{\cdot}m^{-2}{\cdot}Hz^{-1}}$) being the spectral exitance of the exciting star (blackbody) at temperature $T = 20{,}000$ K, close to the value of 20,400 K reported by Van den Ancker et al. (1997). In the equation, $R_\star$ is the radius of the illuminating source, and $D_\star$ is the distance between the illuminating source and NGC 7023. The absorbed power density per frequency $\mathcal{P}(\nu)$ is then given by

$$\mathcal{P}(\nu) = \left(\frac{R_\star}{D_\star}\right)^2 \times u^\circ(\nu; T) \times \mathrm{C_{abs}}(\nu) \times n_\mathrm{C}^{2/3}, \tag{C.2}$$

with C_abs ($\mathrm{m^2}$) as the electronic absorption cross-section of the set of C_{60} cage carbon clusters and n_C ($\mathrm{m^{-3}}$) as the C_{60} cages volume density in the region. Then, the total absorbed power density is written as

$$\int_0^{\nu_\mathrm{ion}} \mathcal{P}(\nu)\, \mathrm{d}\nu, \tag{C.3}$$

with $E_\mathrm{ion} = h\nu_\mathrm{ion}$ as the mean ionisation threshold of C_{60} cages (set to 7.5 eV as mentioned in Appendix A). To obtain the power density detected on Earth, we had to multiply the quantity (C.3) by

$$\frac{1}{4\pi}\left(\frac{R_\triangle}{D_\triangle}\right)^2, \tag{C.4}$$

with $R_\triangle$ as the spatial extension of the observed region of NGC 7023 and $D_\triangle$ as the distance between Earth and NGC 7023. Thus, keeping in mind that the emission spectrum shown in Figure 3(b) is normalised, the spectral power density that should be detected on Earth can be deduced by multiplying the y-axis of Figure 3(b) by the following quantity:

$$\frac{1}{4\pi}\left(\frac{R_\triangle}{D_\triangle}\right)^2 \left(\frac{R_\star}{D_\star}\right)^2 n_\mathrm{C}^{2/3} \int_0^{\nu_\mathrm{ion}} \mathrm{d}\nu\, u^\circ(\nu; T)\mathrm{C_{abs}}(\nu). \tag{C.5}$$

Several distances are involved in (C.5). The distance $D_\triangle$ between Earth and NGC 7023 has been estimated to be around 430 pc Van den Ancker et al. (1997). The spatial extension $R_\triangle$ of the observed region inside NGC 7023 has been determined by the information that the diaphragm aperture is 12″ Sellgren (1984). Thus, the last term in the quantity (C.5) is estimated as

$$\frac{1}{4\pi}\left(\frac{R_\triangle}{D_\triangle}\right)^2 = \frac{1}{4\pi}(\tan 6'')^2 = 6.7 \cdot 10^{-11}\,\mathrm{sr^{-1}}. \tag{C.6}$$

The distance $D_\star$ between the observed region and the exciting binary star has been estimated from Sellgren (1984), where it was indicated that the observed region position is localised at 30″W 20″N relative to the exciting binary star (the distance to the star is then 36″). Assuming that the exciting star and the observed region are in a plane perpendicular to the line of sight, the distance $D_\star$ is obtained from

$$D_\star^2 = (D_\triangle \tan 30'')^2 + (D_\triangle \tan 20'')^2\,, \tag{C.7}$$

thus giving $D_\star = 7.5 \cdot 10^{-2}$pc.

According to Pogodin et al. (2004), the exciting source is a binary star composed of a mass of $10M_\odot$ and a radius of $8R_\odot$ together with a smaller companion with $3.5M_\odot$ mass. Thus, we assumed that the total radius $R_\star$ is around $10R_\odot = 2.3 \cdot 10^{-7}$ pc. Hence the square ratio between $R_\star$ and $D_\star$ entering Eq. C.3 equates

$$\left(\frac{R_\star}{D_\star}\right)^2 = \left(\frac{2.3 \cdot 10^{-7}\ \mathrm{pc}}{7.5 \cdot 10^{-2}\ \mathrm{pc}}\right)^2 = 9.4 \cdot 10^{-12}. \tag{C.8}$$

The integral involved in Eq. C.5 was numerically calculated via the electronic cross-section shown in the left panel of Figure A.2 (Appendix A). For a blackbody at 20,000 K, this integral is equal to $3.9 \cdot 10^{-6}$ W. Therefore, the quantity (C.5) is finally given by

$$1.7 \cdot 10^{-6} \cdot 3.6 \cdot 10^{-6} \cdot n_\mathrm{C}^{2/3} \cdot 6.7 \cdot 10^{-11} = 2.3 \cdot 10^{-27} \cdot n_\mathrm{C}^{2/3}\ \mathrm{W \cdot m^{-2} \cdot sr^{-1}}. \tag{C.9}$$

This value stands for the maximum power density per solid angle detected on Earth and stemming from RF of C_{60} cage carbon clusters illuminated by the binary star HD 200775 at 20,000 K. This value is maximal because HD 200775, the observed region, and the observation point (Earth) are assumed to form a rectangled triangle, and the observed region is at the apex formed by the right angle.

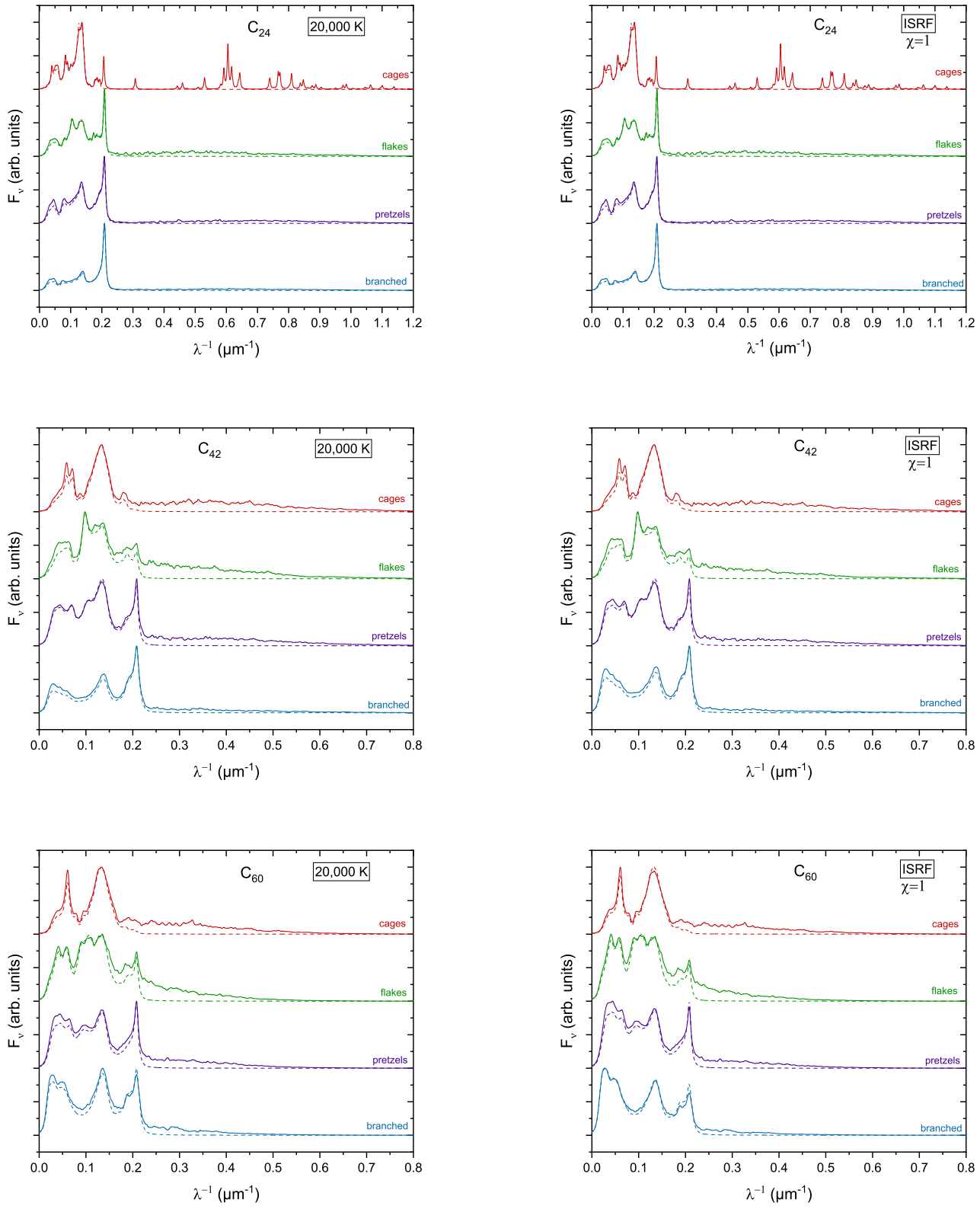

Fig. B.1: Normalised emission intensity spectra from the four structural families of the three carbon cluster samples, as obtained by irradiation from a 20,000 K blackbody (left panels) and the standard interstellar radiation field with $\chi = 1$ (right panels). The spectra with dotted lines were obtained by neglecting RF processes.